International Journal of Modern Physics E
Vol. 25, No. 11 (2016) 1650090 (22 pages)

DOI: 10.1142/S0218301316500907

Effects of isovector scalar meson on neutron star both with and without hyperon

S. K. Biswal*,†,‡, Bharat Kumar*,† and S. K. Patra*,†

*Institute of Physics, Bhubaneswar 751 005, India

†Homi Bhabha National Institute, Training School Complex, Anushakti Nagar, Mumbai 400085, India

‡sbiswal@iopb.res.in

Received 4 July 2016
Revised 12 September 2016
Accepted 13 October 2016
Published 15 November 2016

We study the effects of isovector-scalar (δ)-meson on neutron and hyperon stars. Influence of δ-meson on both static and rotating stars is discussed. The δ-meson in a neutron star consisting of protons, neutrons and electrons, makes the equations of states (EOS) stiffer at higher density, and consequently increases the maximum mass of the star. But induction of δ-meson in the hyperon star decreases the maximum mass. This is due to the early evolution of hyperons in presence of δ-meson.

Keywords: Relativistic mean field theory; EOS; compressibility; neutron star; hyperon star.

PACS Number(s): 26.60.+c, 97.60.Gb, 14.20.Jn

1. Introduction

Neutron star is a venerable candidate to discuss the physics at high density. We cannot create such a high density in a terrestrial laboratory, so a neutron star is the only object, which can provide much information on high-density nature of the matter.[1,2] But it is not an easy task to deal with the neutron star owing to its complex nature, as all the four fundamental forces (strong, weak, gravitational and electromagnetic) are active. High gravitational field makes it mandatory to use general theory of relativity for the study of neutron star structure. Equations of states (EOS) are the sole ingredient that must be supplied to the equation of stellar structure, Tolman–Oppenheimer–Volkoff (TOV) equation, whose output is the mass–radius profile of the dense neutron star. In this case, the nuclear EOS plays an intimate role in deciding the mass–radius of a neutron star. Its indispensable importance attracts the attention of physicists to have an anatomy of the interactions Lagrangian. As the name suggests, a neutron star is not completely made

up neutrons, a small fraction of protons and electrons are also present, which is the consequence of the β-equilibrium and charge neutrality condition.[3] Also, the presence of exotic degrees of freedom like hyperons and kaons cannot be ignored in such high dense matter. It is one of the most asymmetric and dense nuclear objects in nature.

From last three decades,[4,5] the relativistic mean field (RMF) approximation, generalized by Walecka[6] and later on developed by Boguta and Bodmer[7] is one of the most reliable theories to deal with the infinite nuclear matter and finite nuclei. The original RMF formalism starts with an effective Lagrangian, whose degrees of freedom are nucleons, σ-, ω-, ρ- and π-mesons. To reproduce proper experimental observable, it is extended to the self-interaction of σ-meson. Recently, all other self- and crossed interactions including the baryon octet are also introduced keeping in view the extra-ordinary condition of the system, such as highly asymmetric system or extremely high-density medium.[8] Since the RMF formalism is an effective nucleon–meson model, the coupling constants for both nucleon–meson and hyperon–meson are fitted to reproduce the properties of selected nuclei and infinite nuclear matter properties.[6,7,9,10] In this case, it is improper to use the parameters obtained from the free nucleon–nucleon scattering data. The parameters, with proper relativistic kinematics along with the mesons and their properties, are already known or fixed from the properties of a small number of finite nuclei, the method gives excellent results not only for spherical nuclei, but also for well-known deformed cases. The same force parametrization can be used both for β-stable and β-unstable nuclei throughout the periodic table.[11–14]

The importance of the self- and crossed-interactions are significant for some specific properties of nuclei/nuclear-matter in certain conditions. For example, self-interaction of σ-meson takes care of the reduction of nuclear matter incompressibility K_∞ from an unacceptable high value of $K_\infty \sim 600\,\text{MeV}$ to a reasonable number of $\sim 270\,\text{MeV}$,[7,15] while the self-interaction of vector meson ω softens the EOS.[14,16] Thus, it is imperative to include all the mesons and their possible interactions with nucleons and hyperons, self- and crossed terms in the effective Lagrangian density. However, it is not necessary to do so because of the symmetry reason and their heavy masses.[17] For example, to keep the spin-isospin and parity symmetry in the ground state, the contribution of π-meson is ignored[18] and also the effect of heavier mesons is neglected for their negligible contribution. Taking into this argument, in many versions of the RMF formalism, the inclusion of isovector-scalar (δ) meson is neglected due to its small contribution. But recently it is seen[19–24] that the endowment of the δ-meson goes on increasing with density and asymmetry of the nuclear system. Thus, it will be impossible for us to justify the abandoning of δ-meson both conceptually and practically, while considering the high asymmetry and dense nuclear systems, like the neutron star and relativistic heavy ion collision. Recent observation of neutron star-like PSR J1614-2230 with mass of $(1.97 \pm 0.04)M_\odot$[25] and the PSR J0348+0432 with mass of $(2.01 \pm 0.04)M_\odot$[26] reopen the challenge in the dense matter physics. The heavy mass of PSR J0348+0432

($M = 2.01 \pm 0.04 M_{\odot}$) forces the nuclear theorists to re-think the composition and interaction inside the neutron star. Therefore, it is important to establish the effects of the δ-meson and all possible interactions of other mesons for such compact and asymmetry system.

The paper is organized as follows. In Sec. 2, we have outlined a brief theoretical formalism. The necessary steps of the RMF model and the inclusion of δ-meson are explained. The results and discussions are discussed in Sec. 3. Here, we have attempted to explain the effects of δ-meson on the nuclear matter system-like hyperon and proton–neutron stars. This analysis is done for both static and rotating neutron and neutron–hyperon stars. In these calculations, the E-RMF Lagrangian ($G2$ parameter set) is used to take care of all possible self- and crossed interactions.[27] On top of the $G2$ Lagrangian, the δ-meson interaction is added to take care of the isovector channel. The concluding remarks are given in Sec. 4.

2. Theoretical Formalism

From last one decade, a lot of work has been done to emphasize the role of δ-meson on both finite and infinite nuclear matter.[28–31] It is seen that the contribution of δ-meson to the symmetry energy is negative.[32] To fix the symmetry energy around the empirical value ($\sim$30 MeV), we need a large coupling constant of the ρ-meson (g_ρ) value in the absence of the g_δ. The proton and neutron effective masses split due to inclusion of δ-meson and consequently it affects the transport properties of neutron star.[19] The addition of δ-meson not only modifies the property of infinite nuclear matter, but also enhances the spin-orbit splitting in the finite nuclei.[28] A lot of mystery is present in the effects of δ-meson till date. The motivation of the present paper is to study such information. It is to be noted that both the ρ- and δ-mesons correspond to the isospin asymmetry, and a careful precaution is essential while fixing the δ-meson coupling in the interaction.

The effective field theory and naturalness of the parameter are described in Refs. 27, 33–36. The Lagrangian is consistent with underlying symmetries of the QCD. The $G2$ parameter is motivated by E-RMF theory. The terms of the Lagrangian are taken into account up to fourth-order in meson–baryon coupling. For the study of isovector channel, we have introduced the isovector-scalar δ-meson. The baryon–meson interaction is given by[8]

$$\begin{aligned}\mathscr{L} = & \sum_B \overline{\psi}_B (i\gamma^\mu D_\mu - m_B + g_{\sigma B}\sigma + g_{\delta B}\delta.\tau)\psi_B + \frac{1}{2}\partial_\mu\sigma\partial_\mu\sigma \\ & - m_\sigma^2\sigma^2\left(\frac{1}{2} + \frac{\kappa_3}{3!}\frac{g_\sigma\sigma}{m_B} + \frac{\kappa_4}{4!}\frac{g_\sigma^2\sigma^2}{m_B^2}\right) - \frac{1}{4}\Omega_{\mu\nu}\Omega^{\mu\nu} + \frac{1}{2}m_\omega^2\omega_\mu\omega^\mu \\ & \times\left(1 + \eta_1\frac{g_\sigma\sigma}{m_B} + \frac{\eta_2}{2}\frac{g_\sigma^2\sigma^2}{m_B^2}\right) - \frac{1}{4}R^a_{\mu\nu}R^{\mu\nu a} + \frac{1}{2}m_\rho^2\rho^a_\mu\rho^{a\mu}\left(1 + \eta_\rho\frac{g_\sigma\sigma}{m_B}\right) \\ & + \frac{1}{2}\partial_\mu\delta.\partial_\mu\delta - m_\delta^2\delta^2 + \frac{1}{4!}\zeta_0(g_\omega\omega_\mu\omega^\mu)^2 + \sum_l \overline{\psi}_l(i\gamma^\mu\partial_\mu - m_l)\psi_l. \end{aligned} \tag{1}$$

The co-variant derivative D_μ is defined as:

$$D_\mu = \partial_\mu + ig_\omega\omega_\mu + ig_\rho I_3\tau^a\rho^a_\mu, \tag{2}$$

where $R^a_{\mu\nu}$ and $\Omega_{\mu\nu}$ are field tensors and defined as follows:

$$R^a_{\mu\nu} = \partial_\mu\rho^a_\nu - \partial_\nu\rho^a_\mu + g_\rho\epsilon_{abc}\rho^b_\mu\rho^c_\nu, \tag{3}$$

$$\Omega_{\mu\nu} = \partial_\mu\omega_\nu - \partial_\nu\omega_\mu. \tag{4}$$

Here, σ, ω, ρ and δ are the sigma, omega, rho and delta meson fields, respectively, and in real calculation, we ignore the non-Abelian term from the ρ-field. All symbols are carrying their own usual meaning.[8,21]

The Lagrangian equation for different mesons is given by[8]

$$m_\sigma^2\left(\sigma_0 + \frac{g_\sigma\kappa_3\sigma_0}{2m_B} + \frac{\kappa_4 g_\sigma^2\sigma_0^2}{6m_B^2}\right)\sigma_0 - \frac{1}{2}m_\rho^2\eta_\rho\frac{g_\sigma\rho_{03}^2}{m_B} - \frac{1}{2}m_\omega^2\left(\eta_1\frac{g_\sigma}{m_B} + \eta_2\frac{g_\sigma^2\sigma_0}{m_B^2}\right)\omega_0^2 = \sum g_\sigma\rho_B^s, \tag{5}$$

$$m_\omega^2\left(1 + \eta_1\frac{g_\sigma\sigma_0}{m_B} + \frac{\eta_2}{2}\frac{g_\sigma^2\sigma_0^2}{m_B^2}\right)\omega_0 + \frac{1}{6}\zeta_0 g_\omega^2\omega_0^3 = \sum g_\omega\rho_B, \tag{6}$$

$$m_\rho^2\left(1 + \eta_\rho\frac{g_\sigma\sigma_0}{m_B}\right) = \frac{1}{2}\sum g_\rho\rho_{B3}, \tag{7}$$

$$m_\delta^2\delta^3 = g_\delta^2\rho_{3B}^s \tag{8}$$

with $\rho_{3B}^s = \rho_p^s - \rho_n^s$, ρ_p^s and ρ_n^s are scalar densities for the proton and neutron, respectively. The total scalar density is expressed as the sum of the proton and neutron densities $\rho_B^s = \rho_p^s + \rho_n^s$, which is given by

$$\rho_i^s = \frac{2}{(2\pi)^3}\int_0^{k_i}\frac{M_i^* d^3k}{E_i^*}, \quad i = p, n \tag{9}$$

and the vector (baryon) density

$$\rho_B = \frac{2}{(2\pi)^3}\int_0^{k_i} d^3k, \tag{10}$$

where $E_i^* = (k_i^2 + M_i^{*2})^{1/2}$ is the effective energy, k_i is the Fermi momentum of the baryons. M_p^* and M_n^* are the proton and neutron effective masses written as

$$M_p^* = M_p - g_\sigma\sigma_0 - g_\delta\delta^3, \tag{11}$$

$$M_n^* = M_n - g_\sigma\sigma_0 + g_\delta\delta^3, \tag{12}$$

which are solved self-consistently. I_3 is the third component of isospin projection and B stands for baryon octet. The energy and pressure density depend on the effective mass M_B^* of the system, which is first needed to solve these self-consistent

equations and obtain the fields for mesons. Using the Einstein's energy–momentum tensor, the total energy and pressure density are given as[8]

$$\mathscr{E} = \sum_B \frac{2}{(2\pi)^3}\int_0^{k_B} d^3kE_B^*(k) + \frac{1}{8}\zeta_0 g_\omega^2\omega_0^4 + m_\sigma^2\sigma_0^2\left(\frac{1}{2} + \frac{\kappa_3}{3!}\frac{g_\sigma\sigma_0}{m_B} + \frac{\kappa_4}{4!}\frac{g_\sigma^2\sigma_0^2}{m_B^2}\right)$$
$$+ \frac{1}{2}m_\omega^2\omega_0^2\left(1 + \eta_1\frac{g_\sigma\sigma_0}{m_B} + \frac{\eta_2}{2}\frac{g_\sigma^2\sigma_0^2}{m_B^2}\right) + \frac{1}{2}m_\rho^2\rho_{03}^2\left(1 + \eta_\rho\frac{g_\sigma\sigma_0}{m_B}\right)$$
$$+ \frac{1}{2}\frac{m_\delta^2}{g_\delta^2}(\delta^3)^2 + \sum_l \varepsilon_l, \tag{13}$$

and

$$\mathscr{P} = \sum_B \frac{2}{3(2\pi)^3}\int_0^{k_B} d^3kE_B^*(k) + \frac{1}{8}\zeta_0 g_\omega^2\omega_0^4 - m_\sigma^2\sigma_0^2\left(\frac{1}{2} + \frac{\kappa_3}{3!}\frac{g_\sigma\sigma_0}{m_B} + \frac{\kappa_4}{4!}\frac{g_\sigma^2\sigma_0^2}{m_B^2}\right)$$
$$+ \frac{1}{2}m_\omega^2\omega_0^2\left(1 + \eta_1\frac{g_\sigma\sigma_0}{m_B} + \frac{\eta_2}{2}\frac{g_\sigma^2\sigma_0^2}{m_B^2}\right) + \frac{1}{2}m_\rho^2\rho_{03}^2\left(1 + \eta_\rho\frac{g_\sigma\sigma_0}{m_B}\right)$$
$$- \frac{1}{2}\frac{m_\delta^2}{g_\delta^2}(\delta^3)^2 + \sum_l P_l, \tag{14}$$

where P_l and ε_l are lepton's pressure and energy density, respectively.

3. Results and Discussions

Before going to the discussions of our results, we give a brief description of the parameter fitting procedure for g_ρ and g_δ. As it is commonly known, the symmetric energy, E_s, is an important quantity to select the EOS. This value of E_s determines the structure of both static and rotating neutron stars. On the other hand, an arbitrary combination of g_ρ and g_δ with a fixed value of E_s can affect the ground state properties of finite nuclei. Thus, to have a clear picture on the effect of g_δ on hyperon star structure, we have chosen two different prescriptions for the selection of g_δ in our present calculations. (1) In the first method, we have constructed various sets of g_ρ and g_δ keeping E_s fixed. Here, all the other parameters of $G2$ set remain unchanged. The $G2$ set and the combination of g_ρ and g_δ are displayed in Table 1. (2) In the second procedure, we have chosen the g_ρ, g_δ pairs keeping the binding energy constant (experimental binding energy) for finite nuclei. The values of these g_ρ and g_δ are given in Table 1 with other properties of infinite nuclear matter. It is worthy to re-emphasize here that we are not looking for a full-fledged parameter set including the δ-meson coupling, but our aim in this paper is to study the effects of δ-meson coupling on hyperon star and the production of baryon octet. Therefore, after splitting the g_ρ coupling constant into two parts (g_ρ, g_δ) using the first prescription, the results on hyperon star along with the neutron star structures both for static and rotating cases under β-equilibrium condition are discussed in the subsequent Secs. 3.2–3.6. In Sec. 4, we follow the second procedure to get the (g_ρ, g_δ) pairs and applied these to some selective cases.

Table 1. The parameters for $G2$ set are in the upper panel of the table. The nuclear matter saturation properties are in the middle panel and various g_ρ and g_δ combinations are in the lower panel, keeping symmetry energy $E_{\rm sym} = 36.4\,{\rm MeV}$ fixed.

$m_n = 939.0\,{\rm MeV}$	$m_\sigma = 520.206\,{\rm MeV}$	$m_\omega = 782.0\,{\rm MeV}$	$m_\rho = 770.0\,{\rm MeV}$	$m_\delta = 980.0\,{\rm MeV}$	$\Lambda = 0.0$	$\zeta_0 = 2.642$	$\eta_\rho = 0.39$	
$g_\sigma = 10.5088$	$g_\omega = 12.7864$	$g_\rho = 9.5108$	$g_\delta = 0.0$	$k_3 = 3.2376$	$k_4 = 0.6939$	$\eta_1 = 0.65$	$\eta_2 = 0.11$	
$\rho_0 = 0.153 fm^{-3}$	E/A $= -16.07\,{\rm MeV}$	$K_\infty = 215\,{\rm MeV}$	$E_{\rm sym} = 36.4\,{\rm MeV}$	$m_n^*/m_n = 0.664$				
(g_ρ, g_δ)	$(9.510, 0.0)$	$(9.612, 1.0)$	$(9.973, 2.0)$	$(10.550, 3.0)$	$(11.307, 4.0)$	$(12.212, 5.0)$	$(13.234, 6.0)$	$(14.349, 7.0)$

3.1. *Parametrization of g_ρ and g_δ with constant symmetry energy*

It is important to fix g_δ value to see the effects of the δ-meson. The isovector channels in RMF theory come to exist through both the ρ- and δ-mesons couplings. While considering the effects of the δ-meson, we have to take the ρ-meson into account. Since both the isovector channels are related to isospin, one cannot optimize the g_δ coupling independently. Here, we have followed a more reliable procedure by fixing the symmetry energy $E_{\rm sym}$ by simultaneously adjusting different values of g_ρ and g_δ.[19] In general, for most of the nonrelativistic formalism, the symmetry energy $E_{\rm sym}$ is around 30–33 MeV. However, in some specific parametrization like GS4, $E_{\rm sym} = 12.83$ MeV and for PRC45 set it is 51.01 MeV.[65,66] On the other hand, in nonlinear, density-dependent and point-coupling RMF forces, the $E_{\rm sym}$ varies from 26.1 Mev to 44.0 MeV. Here, we have used the well-known $G2$ parametrization, which has a moderate symmetry energy $E_{\rm sym} = 36.4$ MeV. It is to be noted that the symmetry energy plays a crucial role both in finite nuclei and in the EOS, which include the neutron distribution radius in the nucleus and the mass and radius of a neutron star, respectively. For a smaller value of $E_{\rm sym}$, both the relativistic and nonrelativistic forces predict a smaller neutron star mass contrary to the recent observation of about $2M_\odot$. A detailed variation of symmetry energies for Skyrme effective interaction and nonlinear RMF formalism is available in Refs. 65 and 66. Recently, a large number of papers have been devoted to $E_{\rm sym}$ for a definite value, but this is under active discussions.

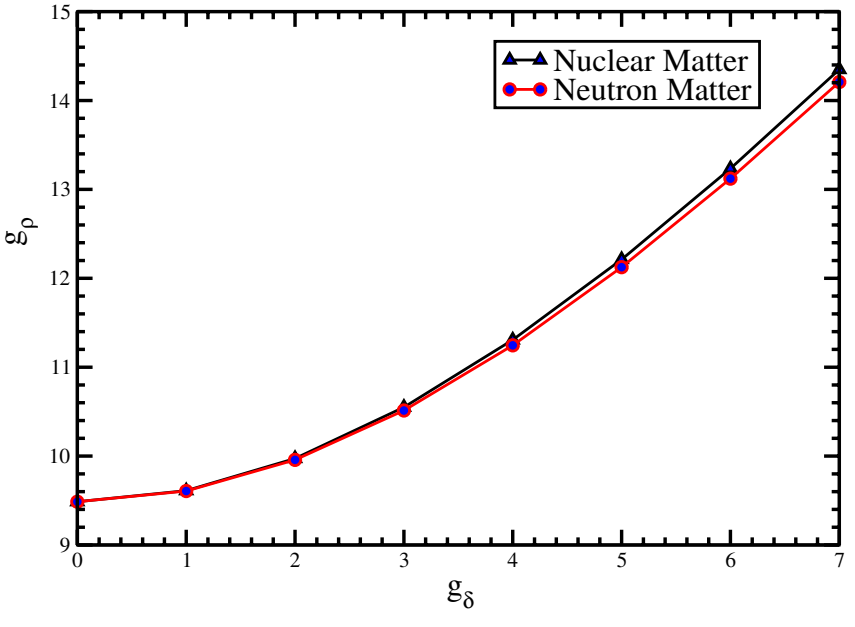

Fig. 1. Variation of g_ρ and g_δ at a constant value of symmetry energy $E_{\rm sym} = 36.4$ MeV for both nuclear and neutron matter.

As it is mentioned earlier, we have added g_δ on top of the $G2$ parameter set. Thus, the symmetry energy of $G2$ parameter $E_{\rm sym} = 36.4\,{\rm MeV}$ is kept constant at the time of re-shuffling g_ρ and g_δ. It is to be noted that we do not want to change the value of $E_{\rm sym}$ of the original $G2$ parameter set with the addition of δ-meson. The $G2$ parameters and the g_δ and g_δ combinations are displayed in Table 1. The nuclear matter properties are also listed in the table (middle panel). For a particular value of $E_{\rm sym} = 36.4\,{\rm MeV}$, the variations of g_ρ and g_δ are plotted in Fig. 1. From Fig. 1, it is clear that as the g_δ increases the g_ρ value also increases, almost linearly, to fix the symmetry energy unchanged. This implies that ρ- and δ-mesons have opposite effect on $E_{\rm sym}$ contribution, i.e., the δ-meson has negative contribution of the symmetry energy contrary to the positive contribution of ρ-meson.

We feel that it is instructive to check the finite nuclear properties with these combinations of g_ρ and g_δ. We have tabulated the binding energy and charge radius of some spherical nucleus in Table 2. From the table, it is clear that binding energy for asymmetric nucleus goes on decreasing with increasing δ-meson and decreasing ρ-meson couplings. However, it is well understood that the scalar δ-meson gives a positive contribution to the binding energy. Thus, the binding energy of asymmetric nuclei should go on increasing with g_δ contrary to the observation seen in Table 2. This happens because of the simultaneous change of (g_ρ, g_δ) pair to keep the constant symmetry energy, i.e., g_ρ is decreasing and g_δ is increasing. As a result, the contribution of ρ-meson, which is negative to the binding energy dominates over the δ-meson effect on binding energy. But in the case of symmetric nucleus, like ^{16}O etc., the effects of both ρ- and δ-mesons are absent due to iso-spin symmetry. A further inspection of Table 2 reveals a slight change in binding energy and charge radius even for symmetric nuclei because of the slight different in density distribution of protons and neutrons, although it is small.

3.2. *Fields of σ, ω, ρ and δ mesons*

The fields of the meson play a crucial role to construct the nuclear potential, which is the deciding factor for all type of calculations in the RMF model. In Fig. 2, we have plotted various meson fields included in the present calculations, such as σ, ω, ρ and δ with g_δ on top of $G2$ parameter set ($G2 + g_\delta$). It is obvious that V_σ and V_ω are opposite to each other, which is also reflected in the figure. This means the positive value of V_ω gives a strong repulsion, which is compensated by the strongly attractive potential of the σ-meson field V_σ. The nature of the curves for V_σ and V_ω is almost similar except the sign. The magnitude of V_σ and V_ω looks almost equal. However, in real (it is not clearly visible in the curve, because of the scale), the value of V_σ is slightly larger than V_ω, which keeps the overall nuclear potential strongly attractive. The attractive V_σ and repulsive V_ω potentials combinely give the saturation properties of the nuclear force. It is worthy to mention that the contributions of self-interaction terms are taken care both in V_σ and V_ω, which are the key quantities to solve the Coester band problem[39] and the explanation

Table 2. Binding energy (MeV) and charge radius (fm) are calculated with various combination of g_ρ and g_δ in $G2 + \delta$. The results are compared with experimental data.[37]

(g_ρ, g_δ)	(9.510, 0.0)	(9.612, 1.0)	(9.973, 2.0)	(10.550, 3.0)	(11.307, 4.0)	(12.212, 5.0)	(13.234, 6.0)	(14.349, 7.0)	
Nucleus	Theory								Expt.
^{16}O (BE)	127.2	127.2	127.2	127.2	127.2	127.2	127.2	127.2	127.6
r_{ch}	2.718	2.718	2.718	2.718	2.718	2.717	2.717	2.716	2.699
^{40} Ca (BE)	341.1	341.1	341.1	341.1	341.1	341.1	341.1	341.1	342.0
r_{ch}	3.453	3.453	3.453	3.453	3.452	3.451	3.450	3.449	3.4776
^{48}Ca (BE)	416.0	415.8	415.2	414.1	412.6	410.7	408.4	405.7	416.0
r_{ch}	3.440	3.439	3.438	3.437	3.435	3.432	3.430	3.427	3.477
^{56}Ni (BE)	480.4	480.3	480.3	480.3	480.3	480.3	480.3	480.2	484.0
r_{ch}	3.730	3.730	3.730	3.730	3.730	3.730	3.730	3.724	
^{58}Ni (BE)	497.2	497.2	497.1	497.0	496.9	496.7	496.5	496.3	506.5
r_{ch}	3.765	3.765	3.763	3.762	3.761	3.758	3.756	3.753	3.775
^{90}Zr (BE)	781.6	781.2	780.6	779.4	777.9	775.9	773.6	770.8	783.9
r_{ch}	4.238	4.238	4.237	4.235	4.233	4.230	4.228	4.225	4.269
^{116}Sn (BE)	981.2	980.7	979.4	977.2	974.1	970.2	965.6	960.3	988.7
r_{ch}	4.604	4.603	4.601	4.598	4.594	4.589	4.584	4.579	4.625
^{118}Sn (BE)	997.6	997.1	995.4	992.7	989.0	984.3	978.7	972.2	1004.9
r_{ch}	4.620	4.619	4.617	4.613	4.610	4.604	4.599	4.594	4.639
^{120}Sn (BE)	1013.9	1013.2	1011.2	1008.0	1003.5	998.0	991.3	983.8	1020.5
r_{ch}	4.627	4.626	4.624	4.620	4.616	4.610	4.605	4.600	4.652
^{208}Pb (BE)	1633.3	1631.4	1625.7	1616.2	1603.0	1586.4	1566.4	1543.5	1636.4
r_{ch}	5.499	5.498	5.497	5.494	5.492	5.489	5.487	5.485	5.501

Table 3. Mass and radius of the neutron star are calculated at different values of g_ρ and g_δ keeping binding energy of ^{208}Pb (1633.296 MeV) constant. The calculated results of $E_{\rm sym}$, $L_{\rm sym}$ and $K_{\rm sym}$ are for nuclear matter at different combinations of (g_ρ, g_δ) pairs.

(g_ρ, g_δ)	$\frac{M}{M_\odot}$	Radius (km)	$E_{\rm sym}$ (MeV)	$L_{\rm sym}$ (MeV)	$K_{\rm sym}$ (MeV)
(9.510, 0.0)	1.980	11.230	36.4	101.0	−7.58
(9.588, 1.746)	1.993	11.246	35.3	98.3	−0.60
(9.896, 3.543)	1.997	11.262	31.7	90.2	20.90
(10.518, 5.742)	2.004	11.294	23.8	72.5	67.07
(11.774, 8.834)	2.018	11.510	6.35	30.6	169.03

of quark–gluon-plasma (QGP) formation within the RMF formalism.[40] The self-interaction of the σ-meson gives a repulsive force at long range part of the nuclear potential, which is equivalent to the three-body interaction and responsible for the saturation properties of nuclear force. The calculated results of V_σ and V_ω are compared with the results obtained from DBHF theory with Bonn-A potential[38] and NL3[13] force.

Figure 2 clearly shows that in the low density region (density $\rho_B \sim 2\rho_0$), both RMF and DBHF theories well matched. But as it increases beyond density $\rho_B \sim 2\rho_0$ (ρ_0 is the nuclear saturation density), both the calculations deviate from each other. The possible reason may be the fitting procedure of parameters in Bonn-A potential

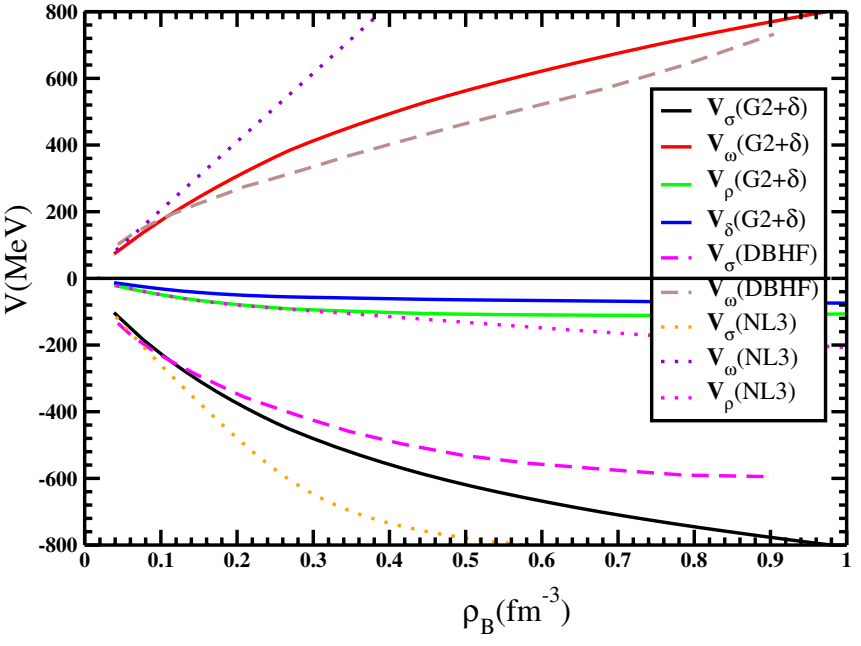

Fig. 2. (Color online) Various meson fields are obtained from the RMF theory with $G2 + g_\delta$ and NL3 parameter sets. The σ-meson field V_σ and ω-meson field V_ω from $G2 + g_\delta$ calculations are compared with the results of DBHF theory[38] and NL3 set.

is up to 2–3 times of saturation density ρ_0, beyond that the DBHF data are simple extrapolation of the DBHF theory. Again, the V_ω and V_σ fields of NL3 are very different from $G2+\delta$ results. The V_ω for NL3 follows a linear path contrary to the results of $G2+\delta$ and Bonn-A. This could be due to the absence of self- and crossed-couplings in NL3 set. The contribution of both ρ- and δ- mesons correspond to the isovector channel. The δ-meson gives different effective masses for proton and neutron because of their opposite isospin of the third component. The nuclear potential generated by the ρ- and δ-mesons are also shown in Fig. 2. We noticed that their contributions are small, but nonnegligible. These nonzero values of V_ρ and V_δ to the nuclear potential have a significant consequence, mostly in compact dense object like neutron or hyperon stars, which will be discussed later in this paper.

3.3. *Energy per particle and pressure density*

The energy and pressure densities as a function of baryonic density ρ_B are known as EOS. These quantities are the key ingredients to describe the structure of neutron/hyperon stars. To see the sensitivity of the EOS, we have plotted energy per particle $(E/\rho_B - M)$ as a function of density for pure neutron matter in Fig. 3. Each curve corresponds to a particular combination of g_δ and g_ρ (taken from Table 1), which reproduces the symmetry energy $E_{\rm sym} = 36.4\,\text{MeV}$ without destabilizing other parameters of $G2$ set. The green line represents for $g_\delta = 0$, i.e., with pure $G2$

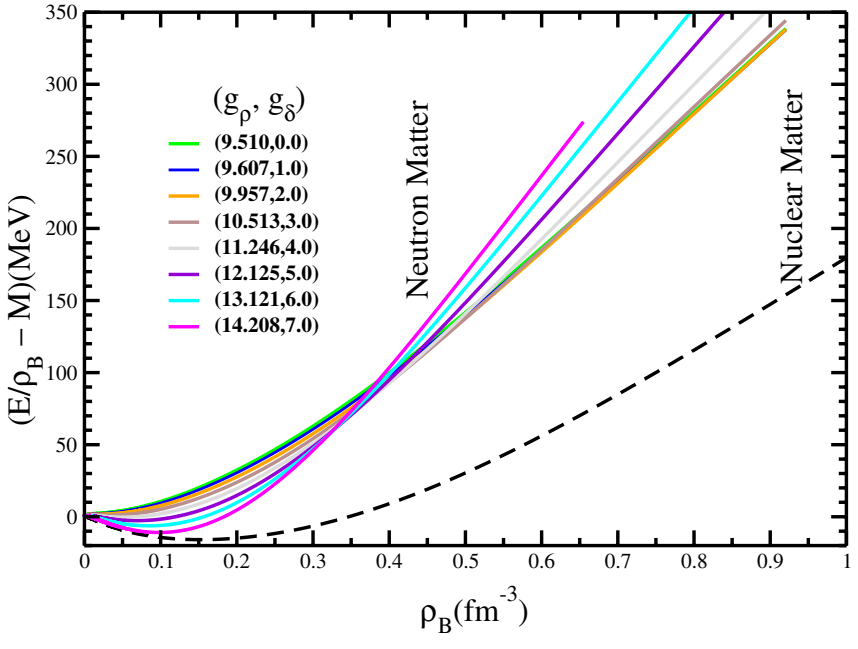

Fig. 3. (Color online) Variation of binding energy per particle with density at various g_ρ and g_δ.

parameter set. Both the binding energy per particle as well as the pressure density increase with the value of g_δ. This process continues till the value of g_δ reaches, at which $E/\rho_B - M$ equals the nuclear matter binding energy per particle. An unphysical situation arises beyond this value of g_δ because the binding energy of the neutron matter will be greater than $E/\rho_B - M$ for the symmetric nuclear matter. In the case of $G2 + \delta$ parametrization, this limiting value of g_δ reaches $g_\delta = 0.7$ after which we do not get a convergence solution in our calculations.

In Fig. 4, we have plotted the variation of energy and pressure densities as a function of ρ_B/ρ_0 for different combinations of g_ρ and g_δ. The enlarged version of energy density in the sub-saturation region is shown in panel (c) of the figure. Similar to other parameter sets of RMF formalism, the $G2 + \delta$ set also deviates from the experimental data. It is to be recalled here that special attention is needed to construct nucleon–nucleon interaction to fit the data at sub-saturation density. For example, the potentials of Friedman and Pandharipande,[41] Baldo–Maieron,[42] DDHF[43] and AFDMC[44] are designed to fit the data in this region. The three-body effect also cannot be ignored in this sub-saturation region of the density.[45] Although the nonlinear interactions fulfilled this demand to some extent,[39,40,46] like Coester band problem,[47] still some further modification of the couplings are needed. In this regard, the RMF calculations with density dependent meson–nucleon coupling[48] and constraining the RMF models of the nuclear matter EOS at low densities[49] are some of the attempts. The mean field approximation is also a major limitation in the region of sub-saturation density. This is because the assumption of classical meson field is not a proper approximation in this region to reproduce precisely the

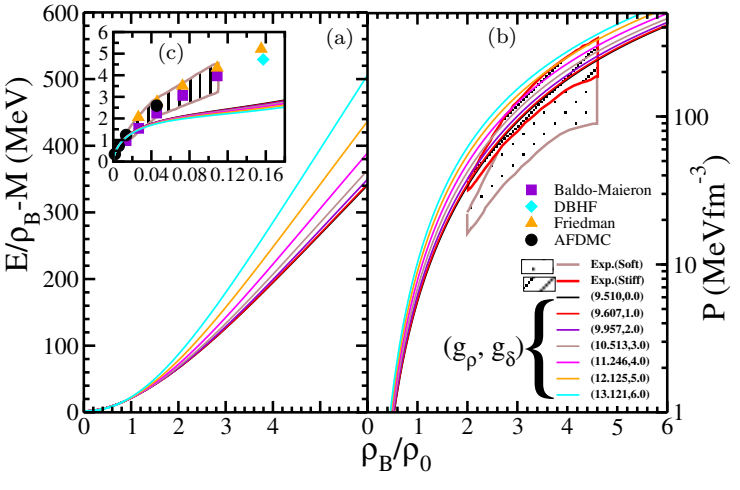

Fig. 4. (Color online) Variation of energy per particle (panel (a)) and pressure density (panel (b)) with ρ_B/ρ_0 at different values of g_ρ and g_δ. The enlarged version of energy per particle for sub-saturation region is in panel (c). The results of other theoretical models like Baldo–Maieron,[42] DDHF,[43] Firedman[41] and AFDMC[44] are also given for comparison.

data. In higher density region, most of the RMF forces reproduce the experimental data quite well and the predictive power of these forces for finite nuclei is in excellent agreement both for β-stable and β-unstable nuclei. The energy and pressure densities with $G2$ set reproduce the experimental data satisfactorily.[50] The variation of pressure density as a function of ρ_B is shown in panel (b) of Fig. 4, which passes inside the stiff flow data at higher density.[51] Also, the δ-meson coupling has significant effect in supersaturation density than the sub-saturation region. All the EOS with different g_ρ and g_δ remain inside the stiff flow data (Fig. 4(b)). In the present investigation, we are more concerned about highly dense neutron and hyperon stars, which are considered to be super-saturated nuclear objects.

3.4. *Stellar properties of static and rotating neutron stars*

The β-equilibrium and charge neutrality are two important conditions to justify the structural composition of the neutron/hyperon stars. Both these conditions force the stars to have ∼90% of neutron and ∼10% proton. With the inclusion of baryons, the β-equilibrium conditions between chemical potentials for different particles

$$\begin{aligned} \mu_p &= \mu_{\Sigma^+} = \mu_n - \mu_e, \\ \mu_n &= \mu_{\Sigma^0} = \mu_{\Xi^0} = \mu_n, \\ \mu_{\Sigma^-} &= \mu_{\Xi^-} = \mu_n + \mu_e, \\ \mu_\mu &= \mu_e, \end{aligned} \tag{15}$$

and the charge neutrality condition are satisfied by

$$n_p + n_{\Sigma^+} = n_e + n_{\mu^-} + n_{\Sigma^-} + n_{\Xi^-}. \tag{16}$$

To calculate the mass and radius profile of the static (nonrotating) and spherical neutron star, we solve the general relativity TOV[52] equations which are written as

$$\frac{dP(r)}{dr} = -\frac{G}{c^2}\frac{[\mathscr{E}(r) + P(r)]\left[M(r) + \dfrac{4\pi r^3 P(r)}{c^2}\right]}{r^2\left(1 - \dfrac{2GM(r)}{c^2 r}\right)} \tag{17}$$

and

$$\frac{dM(r)}{dr} = \frac{4\pi r^2 \mathscr{E}(r)}{c^2} \tag{18}$$

with G as the gravitational constant, $\mathscr{E}(r)$ as the energy density, $P(r)$ as the pressure density and $M(r)$ as the gravitational mass inside radius r. We have used $c = 1$. For a given EOS, these equations can be integrated from the origin as an initial value problem for a given choice of the central density $\mathscr{E}_c(r)$. The value of $r(= R)$ at which the pressure vanishes and defines the surface of the star. In order to understand the effect of δ-meson coupling on neutron star structure, we must also look at what happens to massive objects as they rotate and how this affects the space-time

around them. For this, we use the code written by Stergioulas[53] based on Komastu, Eriguchi and Hachisu (KEH) method (fast rotation)[54,55] to construct mass–radius of the uniform rotating star. One should note that the maximum mass of a static star is less than the rotating stars because when the massive objects rotate they flatten at their poles. The forces of rotation, namely the effective centrifugal force pulls the mass farthest from the center further out creating the equatorial bulge. This pull-away from the center will, in part, counteract gravity, allowing the star to be able to support more mass than its nonrotating star.

We know that the core of neutron stars contains hyperons at very high density ($\sim$7–8 ρ_0) matter. As it is mentioned before, with the presence of baryons, the EOS becomes softer and stellar properties will change. The maximum mass of hyperon star decreases about 10–20% depending on the choice of the meson–hyperon coupling constants. The hyperon couplings are expressed as the ratio between the meson–hyperon and meson–nucleon couplings as

$$\chi_\sigma = \frac{g_{Y\sigma}}{g_{N\sigma}}, \quad \chi_\omega = \frac{g_{Y\omega}}{g_{N\omega}}, \quad \chi_\rho = \frac{g_{Y\rho}}{g_{N\rho}}, \quad \chi_\delta = \frac{g_{Y\delta}}{g_{N\delta}}. \tag{19}$$

In the present calculations, we have taken $\chi_\sigma = \chi_\rho = \chi_\delta = 0.6104$ and $\chi_\omega = 0.6666$.[58] One can find similar calculations for stellar mass in Refs. 59–61. Now, we present the star properties like mass and radius in Figs. 5 and 6. In Fig. 5, we have plotted the mass–radius profile for the proton–neutron star as well as for

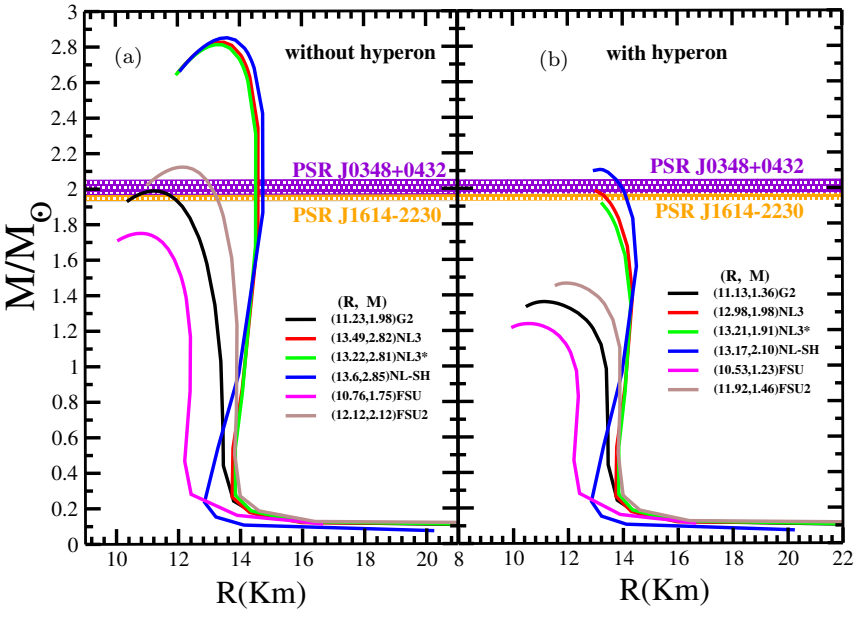

Fig. 5. (Color online) The mass–radius profile for static star with different parametrization like $G2$,[27] NL3,[13] NL3*,[56] NL-SH,[12] FSU[16] and FSU2.[57] (a) is for proton–neutron star and (b) is for the hyperon star. The maximum mass M and the corresponding radius obtained by various parameter sets are given in the parenthesis.

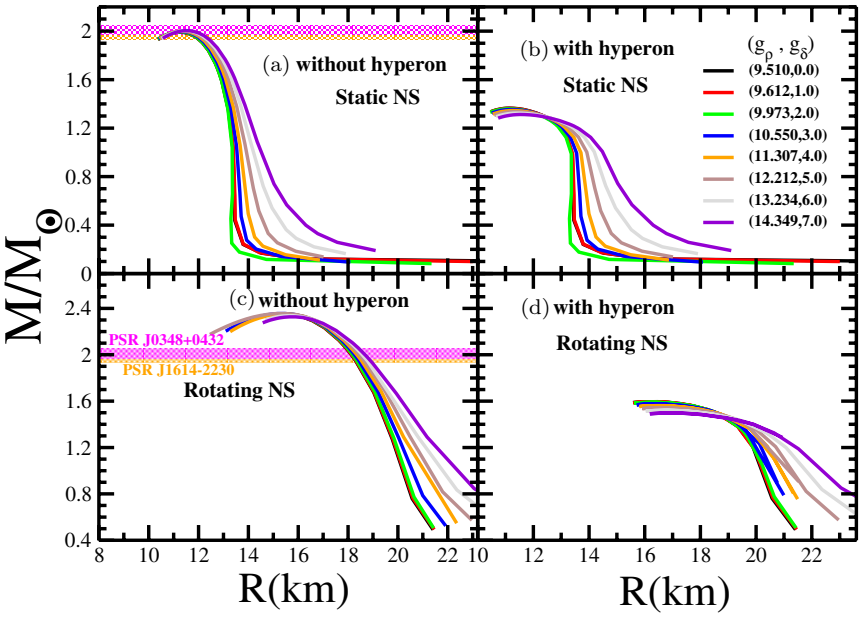

Fig. 6. (Color online) The mass–radius profile of the static and rotating proton–neutron and hyperon stars with various combination of g_δ and g_ρ in $G2+\delta$. (a), (c) is for proton–neutron star and (b), (d) is for the hyperon star. (a), (b) for static and (c), (d) for rotating cases.

the hyperon star using a wide variation of parameter sets starting from the old parameter like NL-SH[12] to the new set of FSU2.[57] The mass–radius profile varies to a great extent over the choice of the parameter. For example, in FSU parameter set,[16] the maximum possible mass of the proton–neutron star is $\sim$1.75 $M_\odot$, while the maximum possible mass for the NL3 set[13] is $\sim$ 2.8 $M_\odot$. These results are shown in the left panel of Fig. 5, while the right panel shows the same things for the hyperon star (the maximum mass and the corresponding radius for different forces are given in the parenthesis).

3.5. *Effects of δ-meson on static and rotating stars*

The main aim of this paper is to understand the effects of δ-meson on neutron stars both with and without hyperons. Figure 6 represents the mass–radius profiles for nonrotating and rotating stars taking into account the presence of with and without hyperons. These profiles are shown for various combinations of g_ρ and g_δ (see Table 1), which we have obtained by fitting the symmetry energy $E_{\rm sym}$ of pure nuclear matter. Analyzing the graphs, we notice a slight change in the maximum mass with g_δ value. That means the mass of the star goes on decreasing with an increase value of the δ-meson coupling in hyperon star. A further inspection of the results reveals that, although the δ-meson coupling has a nominal effects on the

maximum mass of the proto–neutron stars, we get an asymptotic increase in the mass. This asymptotic nature of the curves is more prominent in the presence of hyperons inside the stars. Similar phenomena are also observed in case of rotating stars.

The empirical formula for the relation between maximum frequency $f_{\max}$ with mass of the neutron star for a given EOS is given as[62,63] $f_{\max} \approx 1.22\,\text{kHz}\,\sqrt{M_{\max}^{\text{static}}/M_{\odot}}(R_{\max}^{\text{static}}/10\,\text{km})^{-3/2}$, where $M_{\max}^{\text{static}}$ = maximum static mass and $R_{\max}^{\text{static}}$ = maximum allowed radius for a neutron star. In reality, the neutron stars have a wide range of frequencies due to the fluidity of the stars oscillating in various modes.[64] Among them, the most important modes are the first pressure mode (p_I-mode) and the fundamental mode of the fluid oscillation (f-mode). The empirical formulas for the frequencies of these two modes are $f_f = (0.79 \pm 0.09) + (33 \pm 2)\sqrt{M/R^3}$ and $f_p = 1/M(-1.5 \pm 0.8) + (79 \pm 4)M/R$, respectively, where M and f in km and kHz. The above two relations are obtained by using a wide sample of EOSs.[64]

In the present calculations, we assume the frequency of the rotating neutron star is within the Keplerian frequency limit. At this limit, the spin frequency of the neutron star is equal to the orbital frequency f_{or} (along a circular path on the equator of the NS).[62] If the orbital frequency $f_{\text{or}} > f_K$ (Kepler frequency), then the hydrostatic equilibrium of the NS does not hold good. To make it clear, the Kepler

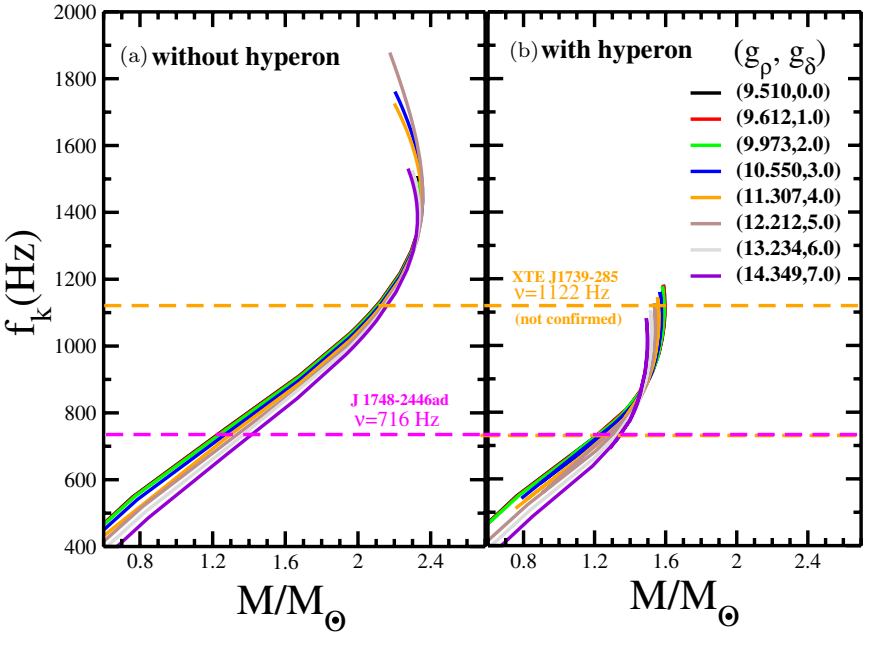

Fig. 7. (Color online) Keplerian frequency of the rotating proton–neutron and hyperon stars with various combination of g_δ and g_ρ in $G2 + \delta$. (a) is for proton–neutron star and (b) is for the hyperon star. The results are obtained from RNS code.[53]

frequency as a function of NS mass is shown in Fig. 7 with and without considering hyperon into account. The results of Fig. 7 are obtained from the RNS code and the expression for the Keplarian frequency, i.e., the maximum frequency obtained from the general theory of relativity can be found in Refs. 53 and 68. In this figure, the variation of f_K is shown as a function of $M/M_\odot$ with various combinations of g_ρ and g_δ which we have already fixed (see Table 1). We noticed a finite effect of g_ρ and g_δ variation on the mass and Keplerian frequency of the pure neutron and hyperon stars.

For quite some time, pulsar B1937+21 with frequency 642 Hz was considered as the fasted spinning NS. However, Hessels *et al.*[70] found even more faster spinning NS pulsar J1748-2446ad at frequency 716.356 Hz. This NS has a mass of $0.14M_\odot$ companion. It is difficult to obtain $0.14M_\odot$ from the EOS at supra-nuclear densities. Our calculations suggest that if pulsar has a mass less than $1.4M_\odot$ than the larger density slope of the symmetry energy at saturation would be excluded. If we consider the neutron star mass to be greater than $2.0M_\odot$ and hyperons are present in it, then the star mass will be $1.6M_\odot$ within the pulsar XTE J1739285 NS.[69]

Here, we analyzed the effects of δ-meson coupling on neutron and hyperon stars. We observed that the mass of the star decreases when hyperons are included in the calculations, as a result, the maximum mass of the star with $G2+\delta$ set becomes much less than $2M_\odot$, the latest observation of a massive neutron star. In summary, the following possibilities are in order:

(i) Since the mass obtained without hyperon for static case is $\sim 2M_\odot$, in this situation one does not need to reduce the mass any more by adding hyperons into it. This can be justifed by assuming that in massive neutron star, there is no hyperon. The absence of hyperons in massive neutron star may not be a convincing explanation because of the highly dense matter in the core of the NS, which favors the production of hyperon. (ii) The rotation of a NS increases the maximum allowed mass. On the other hand, the inclusion of hyperon decreases the mass. In the present case, even if we consider the rotation of the star, it is not sufficient to get the maximum mass $\sim 2M_\odot$ (see Fig. 6(d)). (iii) The third possibility is the effect of δ-meson coupling, which may increase the mass of the hyperon star after its insertion into the model. Although its effect is finite, it is not sufficient to increase the hyperon mass to two solar unit. Thus, the addition of δ-meson may not be sufficient to explain the heavier mass of the NS. (iv) Probably, the fourth possibility may be the most acceptable explanation in which we suggest the modification of the EOS, such that after the addition of hyperon, the mass of the static neutron–hyperon star will be $\sim 2M_\odot$. In particular, the hyperon–meson coupling should be re-investigated to get a proper coupling constants, which allowed the maximum mass $\sim 2M_\odot$ with hyperon. Work in this direction is in progress.[67]

3.6. *Effects of δ-meson on baryon production*

Finally, we want to see the effects of δ-meson coupling on the particle production for the whole baryonic family at various densities in nuclear matter system. The Fermi

energy of both proton and neutron increases with density for their Fermionic nature. After a certain density, the Fermi energy of the nucleon exceeded the rest mass energy of the nucleon (∼1000 MeV), and strange particles (Σ, Λ, Ξ) are produced. As a result, the EOS of the star become soft and give a smaller star mass compared to the neutron star containing only protons, neutrons and electrons. The decrease in star mass in the presence of whole baryon octet can be understood from the analysis of Fig. 8. From the figure, it is clear that δ-meson has a great impact on the production of hyperons. The inclusion of δ-meson accelerates the strange particle production. For example, the evolution of Σ^- takes place at density $\rho_B = 1.75\rho_0$ in the absence of δ-meson. However, it produces at $\rho_B = 1.67\rho_0$ when δ-meson is there in the system. Similarly, analyzing the evolution of other baryons, we notice that although the early production of baryons in the presence of δ-meson is not in a definite proportion to each other, in each case the yield is faster. A significant shifting towards lower density is maximum for heaviest hyperon (Ξ^0) and minimum for nucleon (see Fig. 8). For example, Ξ^- evolves at $\rho_B = 6.5\ \rho_0$ for a non-δ system and $\rho_B \sim 5.0\ \rho_0$ for medium when δ-meson is included. Thus, the δ-coupling has a sizable impact on the production of hyperons like Ξ^-, Ξ^0 and Σ^+.

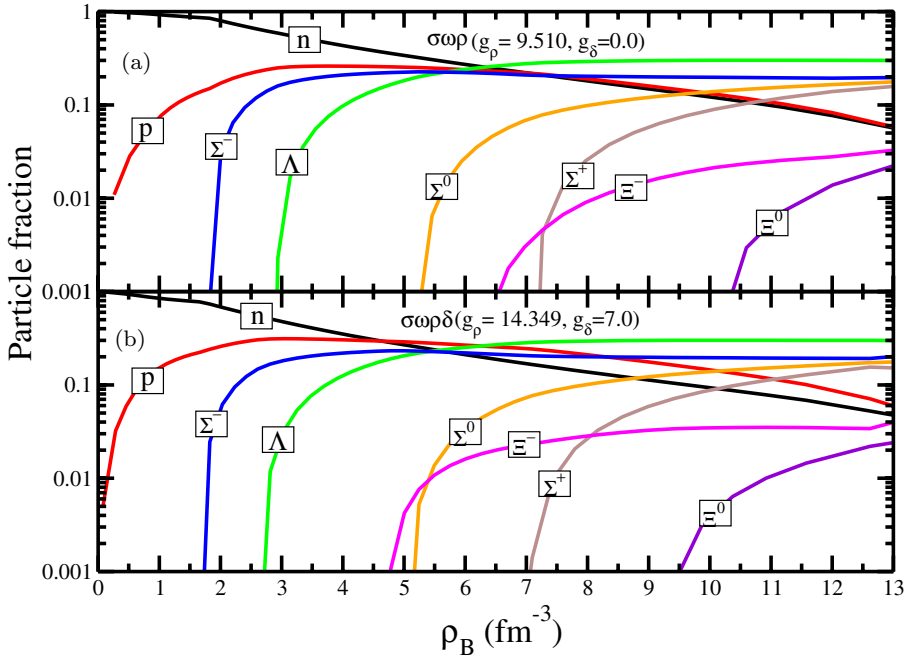

Fig. 8. (Color online) Yield of strange particles as a function of density. The upper panel (a) is with $G2$ parameter set (without taking δ-meson coupling) and the lower panel (b) is with δ-meson coupling.

3.7. *Fitting of g_ρ and g_δ with fixed binding energy and charge radius*

In the previous subsections, we have seen the effects of (g_ρ, g_δ) pair with a constant symmetry energy on the maximum mass and radius of the neutron and hyperon stars. The effects of the (g_ρ, g_δ) pairs are not prominent on the star structure in this method. On the other hand, it affects the bulk properties like binding energy and root mean square radius considerably for asymmetric finite nucleus. In Table 2, we have given the mass and charge radius for some of the selected nuclei. Although all the combination of g_ρ and g_δ are fixed at a constant symmetry energy, the binding of ^{208}Pb differs by 90 MeV in the first and last combination of g_ρ and g_δ. In this subsection, we would like to change the strategy to select the (g_ρ, g_δ) pairs. Here, we have followed the second procedure as we have discussed in the previous subsection, i.e., we find the values of g_ρ and g_δ by adjusting the binding energy and charge radius of ^{208} Pb. Once we get the (g_ρ, g_δ), we use the pair for the calculations of other nuclei of Table 2. Surprisingly, the outcome of binding energy and charge radius matches pretty well with the original calculations. The g_ρ and g_δ combination along with the corresponding mass and radius of a neutron star is given in Table 3. From the table, it is clear that these combinations are also not affecting much the maximum mass and radius of the neutron star. However, the $E_{\rm sym}$, $L_{\rm sym}$ and $K_{\rm sym}$ calculated from the corresponding (g_ρ, g_δ) combinations for nuclear matter change

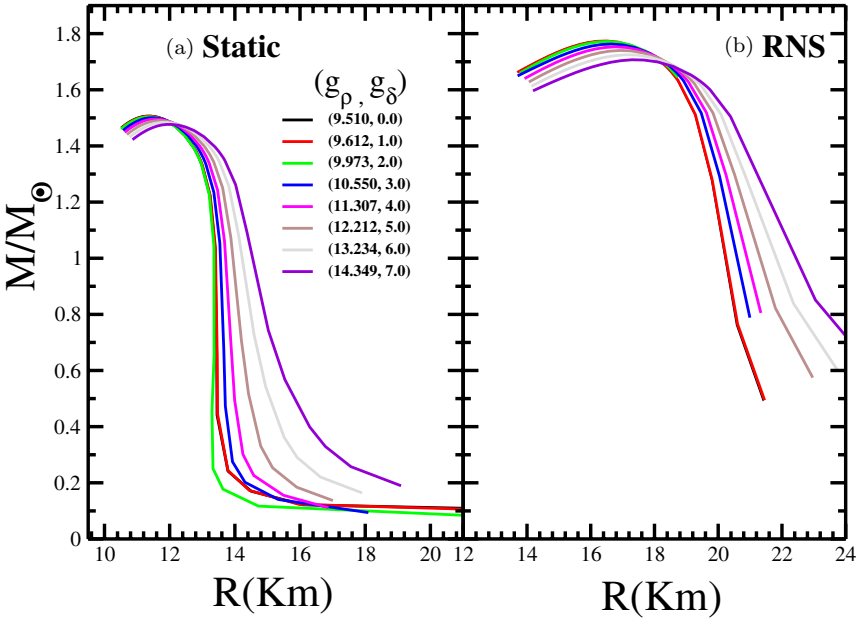

Fig. 9. (Color online) Mass and radius profile of hyperon star with $G2 + \delta$ parameter set, but with different meson–hyperon coupling of Ref. 59.

a lot (see Table 3). We used the hyperon–meson coupling constants of Ref. 59 to evaluate the hyperon star structure. The calculated results for static and rotating hyperon star are plotted in Fig. 9. The maximum mass increases and the radius decreases slightly with the addition of δ-meson to the star system.

4. Summary and Conclusions

In summary, using the effective field theory approach, we discussed the effects of isovector scalar meson on hyperon star. In the inclusion of δ-meson with $G2$ parameter set, we have investigated the static and rotating stellar properties of neutron star with hyperons. We fitted the parameters and saw the variation of g_ρ and g_δ at a constant symmetry energy for both the nuclear and neutron matter. We also used these (g_ρ, g_δ) pairs to finite nuclei and found a large change in binding energy for asymmetric nuclei. Then we re-fitted the (g_ρ, g_δ) pairs keeping binding energy and charge radius fixed for ^{208}Pb and tested the effects for some selected nuclei and reproduced the data similar to the original $G2$ set. With the help of $G2 + \delta$ model, for static and rotating stars without hyperon core, we get the maximum mass of $\sim 2M_\odot$ and $\sim 2.4M_\odot$, respectively. This prediction of masses is in agreement with the recent observation of $M \sim 2M_\odot$ of the stars. However, with hyperon core the maximum mass obtained are $\sim 1.4M_\odot$ and $\sim 1.6M_\odot$ for static and rotating hyperon stars, respectively. In addition, we have also calculated the production of whole baryon octet with variation in density. We find that the particle fraction changes a lot in the presence of δ-meson coupling. When there is δ-meson in the system, the evolution of baryons is faster compared to a non-δ system. This effect is significant for heavier masses and minimum for lighter baryon. Hence, one can conclude that the yield of baryon/hyperons depends very much on the mesons' couplings. One important information is drawn from the present calculations is that the effect of g_δ is just opposite to the effect of g_ρ. As a consequence, many long standing anomaly, such as the comparable radii of ^{40}Ca and ^{48}Ca be resolved by adjusting the (g_ρ, g_δ) pairs properly. Keeping in view the importance of δ-meson coupling and the reverse nature of g_ρ and g_δ, it is necessary to get a new parameter set including proper values of g_δ and g_ρ, and the work is under progress.

References

1. J. M. Lattimer and M. Prakash, *Science* **304** (2004) 536.
2. J. M. Lattimer and M. Prakash, *Phys. Rep.* **442** (2007) 109.
3. N. K. Glendenning, *Astrophys J.* **293** (1985) 470.
4. P. G. Reinhard, *Rep. Prog. Phys.* **52** (1989) 439.
5. P. Ring, *Prog. Part. Nucl. Phys.* **37** (1996) 193.
6. J. D. Walecka, *Ann. Phys.* (*N.Y.*) **83** (1974) 491.
7. J. Boguta and A. R. Bodmer, *Nucl. Phys. A* **292** (1977) 413.
8. B. K. Sharma, P. K. Panda and S. K. Patra, *Phys. Rev. C* **75** (2007) 035808.
9. P. G. Reinhard, M. Rufa, J. Maruhn, W. Greiner and J. Friedrich, *Z. Phys. A* **323** (1986) 13.

10. Y. K. Gambhir, P. Ring and A. Thimet, *Ann. Phys.* (*N.Y.*) **198** (1990) 132.
11. P. G. Reinhard, *Z. Phys. A* **329** (1988) 257.
12. M. M. Sharma, G. A. Lalazissis and P. Ring, *Phys. Lett. B* **312** (1993) 377.
13. G. A. Lalazissis, J. Konig and P. Ring, *Phys. Rev. C* **55** (1997) 540.
14. Y. Sugahara and H. Toki, *Nucl. Phys. A* **579** (1994) 557.
15. A. R. Bodmer, *Nucl. Phys. A* **526** (1991) 703.
16. B. G. Todd-Rutel and J. Piekarewicz, *Phys. Rev. Lett.* **95** (2005) 122501.
17. R. Machleidt, K. Holinde and Ch. Elster, *Phys. Rep.* **149** (1987) 1.
18. L. D. Miller and A. E. S. Green, *Phys. Rev. C* **5** (1971) 241.
19. S. Kubis and M. Kutschera, *Phys. Lett. B* **399** (1997) 191.
20. J. Kotulič Bunta and Štefan Gmuca, *Phys. Rev. C* **70** (2004) 054309.
21. S. K. Singh, S. K. Biswal, M. Bhuyan and S. K. Patra, *Phys. Rev. C* **89** (2014) 044001.
22. M. Oertel, C. Providłncia, F. Gulminelli and Ad. R. Raduta, *J. Phys. G*, *Nucl. Part. Phys.* **42** (2015) 075202.
23. S. K. Singh, S. K. Biswal, M. Bhuyan and S. K. Patra, *J. Phys. G* **41** (2014) 055201.
24. X. Roca-Maza, X. Viñas, M. Centelles, P. Ring and P. Schuck, *Phys. Rev. C* **84** (2011) 054309.
25. P. B. Demorest, T. Pennucci, S. M. Ransom, M. S. E. Roberts and J. W. T. Hessels, *Nature* (London) **467** (2010) 1081.
26. J. Antoniadis *et al.*, *Science* **340** (2013) 6131.
27. R. J. Furnstahl, B. D. Serot and H.-B. Tang, *Nucl. Phys. A* **615** (1997) 441.
28. F. Hofmann, C. M. Keil and H. Lenske, *Phys. Rev. C* **64** (2001) 034314.
29. B. Liu, V. Greco, V. Baran, M. Colonna and M. Di Toro, *Phys. Rev. C* **65** (2002) 045201.
30. D. P. Menezes and C. Providência, *Phys. Rev. C* **70** (2004) 058801.
31. A. Sulaksono, P. T. P. Hutauruk and T. Mart, *Phys. Rev. C* **72** (2005) 065801.
32. S. K. Singh, M. Bhuyan, P. K. Panda and S. K. Patra, *J. Phys. G* **40** (2013) 085104.
33. R. J. Furnstahl, B. D. Serot and H. B. Tang, *Nucl. Phys. A* **598** (1996) 539.
34. H. Müller and B. D. Serot, *Nucl. Phys. A* **606** (1996) 508.
35. R. J. Furnstahl and B. D. Serot, *Nucl. Phys. A* **671** (2000) 447.
36. R. Machleidt and D. R. Entem, *Phys. Rep.* **503** (2011) 1.
37. Available at: http://www.nndc.bnl.gov/.
38. R. Brockmann and R. Machleidt, *Phys. Rev. C* **42** (1990) 1965.
39. B. B. Sahu, S. K. Singh, M. Bhuyan, S. K. Biswal and S. K. Patra, *Phys. Rev. C* **89** (2014) 034614.
40. S. K. Biswal, S. K. Singh, M. Bhuyan and S. K. Patra, *Braz. J. Phys.* **45** (2015) 347.
41. B. Friedman and V. R. Pandharipande, *Nucl. Phys. A* **361** (1981) 502.
42. M. Baldo and C. Maieron, *Phys. Rev. C* **77** (2008) 015801.
43. J. Margueron, H. Sagawa and K. Hagino, *Phys. Rev. C* **77** (2008) 054309.
44. S. Gandolfi, A. Yu. Illarionov, S. Fantoni, F. Pederiva and K. E. Schmidt, *Phys. Rev. Lett.* **101** (2008) 132501.
45. Steven C. Pieper, V. R. Pandharipande, R. B. Wiringa and J. Carlson, *Phys. Rev. C* **64** (2001) 014001.
46. J.-I. Fujita and H. Miyazawa, *Prog. Theor. Phys.* **17** (1957) 360.
47. F. Coester, S. Cohen, B. Day and C. M. Vincent, *Phys. Rev. C* **1** (1970) 769.
48. S. Typel and H. H. Wolter, *Nucl. Phys. A* **656** (1999) 331.
49. M. D. Voskresenskaya and S. Typel, *Nucl. Phys. A* **887** (2012) 42.
50. P. Arumugam, B. K. Sharma, P. K. Sahu, S. K. Patra, Tapas Sil, M. Centelles and X. Viñas, *Phys. Lett. B* **601** (2004) 51.
51. P. Danielewicz, R. Lacey and W. G. Lynch, *Science* **208** (2002) 1592.

52. J. R. Oppenheimer and G. M. Volkoff, *Phys. Rev.* **55** (1939) 374; R. C. Tolman, *Phys. Rev.* **55** (1939) 364.
53. N. Stergioulas and J. L. Friedman, *Astrophys. J.* **444** (1995) 306; N. Stergioulas, Rapidly rotating neutron star, Available at: http://www.gravity.phys.uwm.edu/rns/; N. Stergioulas, *Living Rev. Relativ.* **6** (2003) 3.
54. H. Komatsu, Y. Eriguchi and I. Hachisu, *Mon. Not. R. Astron. Soc.* **237** (1989) 355.
55. H. Komatsu, Y. Eriguchi and I. Hachisu, *Mon. Not. R. Astron. Soc.* **239** (1989) 153.
56. G. A. Lalazissis, S. Karatzikos, R. Fossion, D. Pena Arteaga, A. V. Afanasjev and P. Ring, *Phys. Lett. B* **671** (2009) 36.
57. W.-C. Chen and J. Piekarewicz, *Phys. Rev. C* **90** (2014) 044305.
58. N. K. Glendenning and S. A. Moszkowski, *Phys. Rev. Lett.* **67** (1991) 2414.
59. N. K. Glendenning, *Compact Stars*, 2nd edn. (Springer, New York, 2000).
60. S. Weissenborn, D. Chatterjee and J. Schaffner-Bielich, *Nucl. Phys. A* **881** (2012) 62; S. Weissenborn, D. Chatterjee and J. Schaffner-Bielich, *Phys. Rev. C* **85** 065802 (2012).
61. L. L. Lopes and D. P. Menezes, *Phys. Rev. C* **89** (2014) 025805.
62. P. Haensel, M. Bejger, M. Fortin and L. Zdunik, arXiv:1601.05368v2 [astro-ph.HE].
63. P. Haensel, A. Y. Potekhin and D. G. Yakovlev, *Neutron Stars 1, Equation of State and Structure* (Springer, New York, 2007).
64. O. Benhar, V. Ferreri and L. Gualtieri, *Phys. Rev. D* **70** (2004) 124015; C. H. Lenzi, M. Malheiro, R. M. Marinho, C. Providencia and G. F. Marranghello, arXiv:0810.4848v4 [gr-qc].
65. L. W. Chen, C. M. Ko and B.-A. Li, *Phys. Rev. C* **76** (2007) 054316.
66. M. Dutra, O. Lourenco, J. S. Sa Martins, A. Delfino, J. R. Stone and P. D. Stevenson, *Phys. Rev. C* **85** (2012) 035201.
67. S. K. Patra, B. Kumar and S. K. Singh (in preparation).
68. N. K. Glendenning and F. Weber, *Phys. Rev. D* **50** (1994) 3836.
69. P. Kaaret *et al.*, *Astrophys. J.* **657** (2007) L97.
70. J. W. Hessels, S. M. Ransom, I. H. Stairs, P. C. C. Freire, V. M. Kaspi and F. Camilo, *Science* **311** (2006) 1901.